Improved Ant Colony Optimization Algorithm based Feature Selection for Remote sensing images in Land cover area

Mr. LAKSHMISHA S K[1], IMPA B H[2], KARTHIK B U[3], Dr. LAXMI SINGH[4]

[1,2]Department of CSE, Presidency University, Bengaluru, India
[3]Department of ECE, Presidency University, Bengaluru, India.
[4]Department of ECE, Rabindranath Tagore University(RNTU), Bhopal India
E-mail: [1]lakshmisha.sk@presidencyuniversity.in, [2]impa@presidencyuniversity.in,
[3]karthikbu1994@gmail.com[4]laxmi15singh@gmail.com

ABSTRACT

In recent times,an important task for comprehending the usefulness of the process of identifying and keeping track of a location's physical qualities in the scene categorization of a remote sensing image has been widely used in many fields. Due to the close association between the scene content in a remote sensing image and the spatial relationship characteristics of CNNs, they have been significantly hampered by the absence of big datasets with accurate annotations. Using such a large dataset for direct training, on the other hand, can result in the network overfitting to noisy input. Therefore, it is necessary to remove noise and enhance the remote sensing image classification of the network. In this work, the remote sensing scene images are enhanced from two datasets, namely the AID and WHU-RS datasets, and the performance is analysed using normalisation of pre-processing. The image is effectively extracted and selected by applying VGG-19 and IACO. Finally, LSTM for effective remote sensing image detection and classification When compared to existing models, the proposed work performed better in remote scene image classification. The experimental results achieved higher recognition accuracy for the AID (96.79%) and WHU-RS (94.79%) of the remote sensing classification.

Key words:*Aerial Image Detection (AID), IACO, Normalization, Remote Sensing Image Classification, VGG – 19*

1.INTRODUCTION

In recent years, we can measure the Earth's surface with finely defined functional structures due to the abundance of high-resolution remote sensing photos that have been available as a result of the quick development of satellite imaging technology [1]. High-resolution remote sensing images are the fundamental data for spatial information technologies in geographic information systems, global positioning satellite systems, and the basic and strategic information resources of the country [2]. The growth of remote sensing satellites, imaging radars, and unmanned aerial vehicle technology further illustrates the development trend of fine resolution, multi-source, increased range, and quantitative data [3]. Numerous studies have been conducted on the interpretation of aerial photographs, and the essential issue that seeks to classify a large number of photos without human interaction is remote sensing scene classification [4]. However, remote sensing scene classification faces a significant problem due to the complex contents of the high-resolution images.

In general, the three primary groups of remote sensing scene classification techniques are low-level techniques, mid-level techniques, and high-level system techniques [5–6]. The low-level techniques are used to discriminate between the various classes of scene in the function and to leverage custom properties like spectral, texture, and structures [7]. In order to gather useful visual data for scene classification, high-level methods based on deep learning techniques are often used [8–9]. The local characteristics retrieved from manually created models serve as the encoding for mid-level visual representation, which is another requirement for mid-level approaches [10]. In addition, a variety of classification techniques are used to identify the system's sensing image. The hand-crafted feature extraction with the classifier is a fundamental component of traditional scene categorization methods [11–12]. Color histograms, gray-level co-occurrence matrices, scale-invariant feature transforms, histograms of directed gradients, local binary patterns, and other manual characteristics are examples of common visual

features. Processing photos with complex scenes is challenging since hand-crafted features always result in weaker feature representation [13]. The capacity of convolutional neural networks (CNNs) to learn powerful features has been dramatically enhanced depending on the execution of computer vision tasks [14–15]. The proposed technique addresses the current difficulties in identifying a remote sensing scene image from the natural scene images that are overlapping and of poor quality. As a result, this work focuses mainly on the feature selection and classification of the remote sensing scene images. The main contribution of the research as given as follows:

- The improved ant colony optimization (IACO) and the classification features are selected during classification by utilising heuristic knowledge. In this, features provide the right parameters to create quick convergence and avoid premature convergence, which increases the classification accuracy.
- Furthermore, ACO-based feature selection is used for removing redundant features from hybrid features. Because redundant features exist in the feature set, they affect the classification. The developed IAOC efficiently classifies remote sensing images.

2. Literature survey:

For classification, Xiaolei Zhao et al. [16] presented residual dense based (RDB) on station spatial attention. In this attention function, multiple RDBs were coupled to form an RDN that integrated multi-layer convolutional properties, including dense connection and residual connection. In order to decrease redundant information in the function, extract more precise features, and enhance feature representation capabilities, channel-spatial attention was also applied after each RDB by focusing on the advantageous aspects of images in both the channel and spatial dimensions. As a result, it exhibits higher feature learning capabilities since it completely leverages the information from the convolutional layer, even though it is challenging for the system to interpret images with complex scenes.

Ran Cao *et al.* [17] introduced self-attention-based deep feature fusion (SAFF), which was used to classify remote sensing scene images. The deep layer components of the remote sensing scene classification were aggregated, and the feature fusion was used to emphasize the weights of the complicated elements. Furthermore, this function includes three primary phases, the first of which is the extraction of convolutional features from the pre-trained model based on two concepts: spatial-wise weighting and channel-wise weighting. Second, SAFF is intended to stress the significance of the features that do not occur while maximizing the spatial and channel responses. Additionally, with a limited pre-trained model and visual attention mechanisms, the classifiers were able to successfully avoid overfitting and demonstrate the usefulness and efficiency of the remote sensing scene classification scheme.

Lin Bai *et al.* [18] demonstrated a novel, portable multi-scale depth-wise network (MSDWNet) for remote sensing scene image classification that combines ESPA-MSDW-effective Net's spatial pyramid attention (ESPA). By enlarging the receptive field of convolutions with a low model parameter and good function accuracy, the system's MSDW convolution was proposed to extract multi-scale features from RSIs. A spatial pyramid structure and 1-D convolution are also used by the ESPA module to extract additional spatial information and lessen the complexity of the channel attention mechanism, respectively, which was designed to extract structural features in the RSIs of the system. Therefore, it is essential to create a top-notch RSI scene categorization framework, even though it requires a lot of time and computational resources to perform.

Rao Muhammad Anwer et al. [19] represented the fusion of several deep colour models for remote sensing image classification and aerial scene classification (AID) using colour representations. The deep models were typically pre-trained using raw RGB pixel values as input and a sizable generic object recognition dataset (Image-Net). Additionally, they show how effectively the deep learning framework and the system's information-theoretic compression strategy operate when numerous colour features are combined. Therefore, this system would contribute to improving scene sensing classifications, but it is constrained by the hand-crafted features' limited expressive potential.

Zhicheng Zhao *et al.* [20] introduced the Enhanced Attention Model (EAM) to enhance

deep neural networks' capacity for feature extraction and generalisation in the classification of remote sensing data. The attention module of the model-based Res-Net is inserted after the convolution layer to determine the function's weight in the original CNN feature map. Additionally, the EAM, which is based on two main sections, namely the enhanced channel attention module and the enhanced spatial attention module, might be widely employed to improve the representational capability of CNNs. It partially solves the issues with scene classification in remote sensing photos with numerous small objects and intricate backdrops. However, significant information is lost during multilayer convolution and pooling, making it difficult for the recovered features to accurately represent targets.

Ref no	Method	Dataset	Result
21	Custom CNN model for classification	EuroSAT	Accuracy (88.21%).
22	Resnet for Feature extraction and SVM for classification	UC Merced Land Use (UCM)	Accuracy (95.71%)
23	Multicolumn stacked denoising sparse Autoencoder (SDSAE) and Fisher vector (FV) for classification	UC Merced and RSSCN7	Accuracy of 92.7% for UCM and 90.4% for RSSCN7
24	Support Vector Machine and Linear Discriminatory Analysis	UCM, Sydney dataset	Accuracy of 80.33% for UCM and 90.% for Sydney dataset
25	CNN and ELM	UCM	Accuracy of 95.62%
26	Caffenet and fine-tuning	UCM	Accuracy of 95.48%
27	Unsupervised feature learning m based on spectral clustering and Bag-of-Visual-Words	WHU-RS	Accuracy of 90.26%
28	Multi-scale completed local binary pattern (MS-CLBP) features and a Fisher vector (FV)	1. UCM 2. 19-class satellite scene dataset	Accuracy of 94.32% for UCM and Accuracy of 93% for 19-class satellite scene dataset
29	Saliency-guided Sparse Filter for Convolutional Neural Networks (SSF-CNN)	1. UCM 2. AID	Accuracy of 88.91% for UCM and Accuracy of 79.57%
30	Convolution Neural Networks-Auto Encoder (CNN-AE)	UCM	Accuracy of 93.90%

Table 1: Literature review

From the table 1, we can analyse that the accuracy is still low, so we propose an effective algorithm for classification

3. Proposed Methodology:

In this research, the remote sensing image scene detection and classification are performed using an improved ant colony optimization algorithm. Initially, scene image data were collected from two datasets, AID and WHU-RS, and effective feature extraction and selection were carried out. Finally, LSTM classifiers are used for image classification. The block diagram of the improved ant colony optimization is shown in Figure 1.

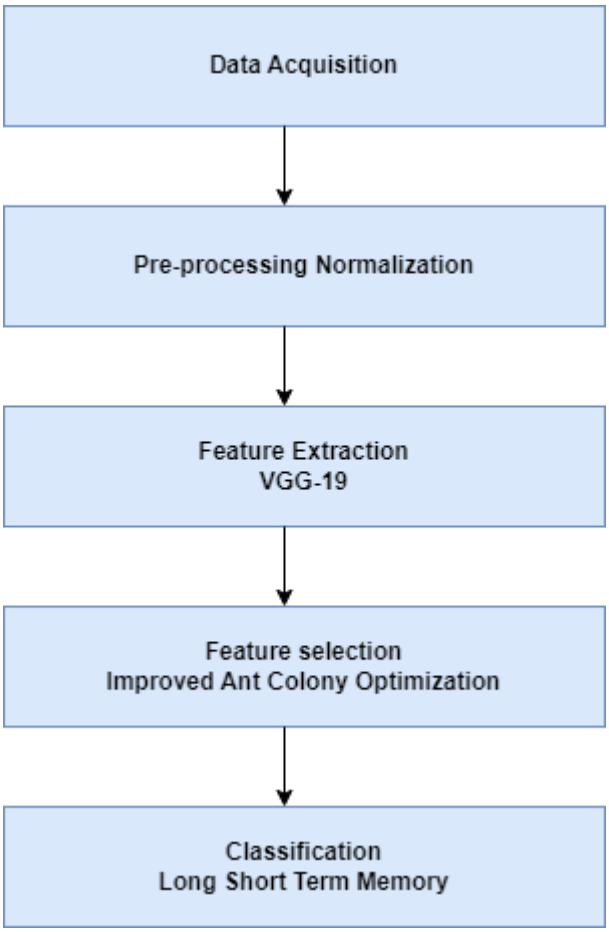

Figure 1. The block diagram of feature selection based on IACO- LSTM.

3.1 Data Acquisition:

The Aerial Image Collection (AID) is a sizable dataset for the classification of aerial photographs that was gleaned from Google Earth. It comprises over 10,000 600 x 600-pixel photos with an 8–0.5 m-pixel resolution. There are around 220–420 photos in each of the 30 scenario categories in the dataset. The dataset contains many types that are very similar to one another, and because it was collected at multiple times and locations, the disparities across the categories are greater.

airport

Figure 2 The sample of AID dataset

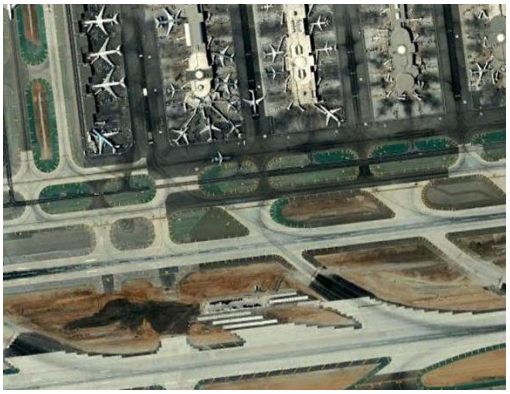

Figure 3. The sample of WHU – RS dataset

The WHU-RS dataset also included data gathered from images on Google Earth. 19 courses have been given 1005 photos. The photos have a high spatial resolution with a pixel size of 600 x 600. Each class is represented by at least 50 photos. The pictures in this dataset provide aerial views of various locations on Earth. The combined AID and WHU-RS dataset has so far been heavily utilized in research studies of various aerial remote scene image classification techniques. The sample AID with WHU-RS datasets are shown in Figures 2 and 3.

3.2 Data Pre-processing using Normalization:

Pre-processing is an important step after data acquisition. Basically, this includes image cropping after radiometric and geometric corrections. The data used in this study has previously undergone geometric and radiometric adjustments. The normalization approach, where bis is the size of the dimension of the plane picture, is used to simplify the work of feature extraction and classification. As a result, standard planes of dimension are not substantially filled in feature relationship adaptive normalization. The image is normalized and centered, with one dimension covered based on the feature ratio. The pre-processed remote sensing images are shown in Figure 4, and the width of the image is marked by U2, and its height is represented by V2, assuming that the plane is square and that X is the length of each side. The feature ratio is represented by equation (1).

$$F_2 = \left\{\frac{U_2}{V_2}, if\ U_2 < V_2, \frac{U_2}{V_2}\right\}, Otherwise \quad (1)$$

Figure 4: The pre-processed image of remote sensing scene.

In this condition, we first establish the mapping coordinates for various normalization techniques, followed by the interpolation of the pixel data. Backward and forward mapping, moment and slant normalizing, and nonlinear normalization are all examples of linear normalization. The transformations ratio, which is denoted by σ $and\gamma$ is determined by equation (2) and (3),

$$\sigma = \frac{U_2}{U_1}$$

(2)

And

$$\gamma = \frac{V_2}{V_1}$$

(3)

In this methodology, the term "normalization of moments" refers to the transformation of a picture that is linear without rotation and size and that will help enhance the remote sensing feature pre-processing function.

3.3 Feature Extraction using VGG- 19:

Following pre-processing, feature extraction is the most difficult task for improving the spatial composition of the remote sensing scene image. Convolutional neural networks, such as the well-known VGG network, have been widely used to address these problems in this order. In the convolutional layers of the Alex Net network, modest filters (33) are used instead of massive filters (1111 and 55). In order to increase the VGG network's capacity for nonlinear mappings, minimise the number of parameters, and broaden the receptive field, these modifications are necessary. Due to the VGG-19 network's remarkably effective image classification capabilities and straightforward structural design, it has recently become widely employed in remote sensing scene categorization. Convolution layers are used for feature extraction during the training phase, and max-pooling layers connected to a few convolution layers are used to reduce the dimensionality of the features. During the first convolution layer, 64 kernels (33 filter sizes) are used to extract features from the input image. The general architecture of the VGG-19 feature extraction model is shown in Fig. 4.

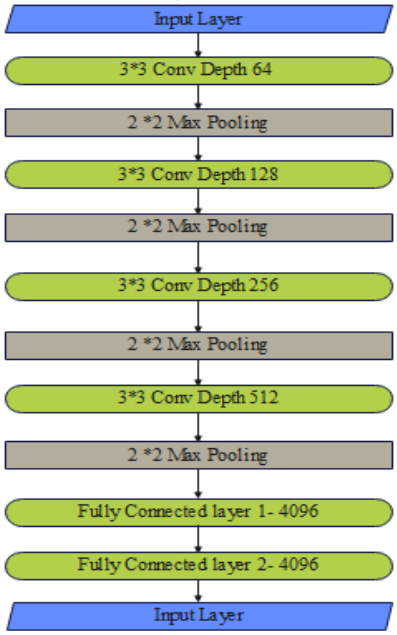

Figure 5 The general architecture of VGG – 19 feature extraction.

Additionally, it is much faster and more accurate than conventional, handcrafted feature-based approaches. Despite stacking numerous convolutional layers, the VGG-19 network lacks the ability to represent remote sensing scene images globally. However, the global information of remote sensing images cannot be accurately modelled by the VGG network with its small receptive fields. To attain enough precision, it also requires a lot of parameters and floating-point computations.

3.4 Feature Selection using Improved Ant Colony Optimization:

One of the most important pre-processing procedures in the classification task is feature selection. Utilizing all of those features in the model-building process will take a lot of time, and the categorization result will suffer significantly because certain features are pointless or even deceptive. A feature selection technique is the most needed part of the function in order to select the most useful features from

the initial feature set without compromising the classifier's quality. Typically, a threshold is manually specified, and features with values over the barrier are chosen because they are thought to be more informative. In this order, iteration and the improved ant colony optimization were proposed, with several ants building whole solutions by utilising their heuristic knowledge of the function. Each ant advances from a state to a state, which corresponds to a more thorough intermediate solution, during each iteration of the algorithm.According to the following equation (4) formula, the K^{th}ant from state r to state s is chosen from the list of unvisited states that J_r^khas memorised:

s

(4)

Additionally, the K^{th}ant moves from state r to state s with the probability of $P_k(r,s)$, are equation (5)

$$P_k(r,s) = \begin{cases} \frac{\tau\,(r,u)^{\alpha}.\eta(r,u)^{\beta}]}{\sum_{u\in J_r^k}\tau\,(r,u)^{\alpha}.\eta\,(r,u)^{\beta}} \\ 0, \qquad otherwise \end{cases} if\ s \in J_r^k \quad (5)$$

Here, the transition probability is denoted by$P_k(r,s)$, the pheromone concentration τ (r, u) between $states\ r$ and u in the i th population η (r, u) is denoted by $(r,s)$and the length of the trail between states r and u is denoted by$(r,s).J_r^k$ is the collection of unexplored states for the K^{th}ant in the ith population; and are control parameters; and q is a uniform probability between [0, 1].

In general, it is challenging to choose the right parameter values to develop an improved ACO algorithm with quick convergence and avoid premature convergence. In order to enhance the ACO algorithm, a multi-population technique is employed. With this tactic, elite ants and common ants will be separated. The elite ants can access solution archives for information, and they can produce solutions by using a probability selection technique and a Gaussian kernel function. In order to prevent settling for a local optimum value, the common ants are employed to produce new solutions at a slower rate by adopting a single Gaussian function and the average value of each dimension. The following is a description of the normal ant's Gaussian function.

$$f_N^i(x) = \frac{1}{\sigma_i N\sqrt{2\pi}} e^{\frac{-(x-\mu_i N)^2}{2\sigma_{i.N}^2}} \quad (6)$$

$$\mu_{i,N} = \sum_{K=1}^{K} S_i, K \quad (7)$$

$$\sigma_{i,N} = \varepsilon_N = \sum_{e=1}^{K} \frac{|S_i, e-\bar{S_i}|}{K-1} \quad (8)$$

Where the estimated standard deviation, $\mu_{i,N}$, and $\sigma_{i,N}$the Gaussian function for normal ants in the i^{th} dimension,$f_N^i(x)$, are all present. Si is the average value of solutions in the i^{th} dimension, while $\varepsilon_N$is a constant used to regulate the common ants' pace of convergence. Therefore, common ants can efficiently expand the search area and improve the capacity to explore globally.

Additionally, the fitness function's design optimizes the likelihood of heuristic path transitions for enhanced capacity. To raise the pheromone value for the particular path and prevent the algorithm from reaching a local optimum, a two-stage pheromone update strategy is used to find the best feature subset. The subset dimension is the smallest, and the accuracy of classification through the subset is the highest.

3.5 Fitness Function of IACO:

The evaluation of each ant's feature subset is an important step in the ACO feature selection method. To assess the pros and cons of the selection features, or the path taken by the ants, a fitness function is created. Both classification accuracy and classification efficiency must be taken into account for the classifier to produce the best results in terms of classification. As a result, the fitness function ought to make the chosen feature subset's feature dimensions smaller while improving classification accuracy. The definition of the fitness function is given in equation (9).

$$F = \omega FPR + (1-\omega)\frac{d}{D} \quad (9)$$

Where, ω the weights between the feature dimensions and the classification performance of

the classifier are balanced using. Moreover, the dimension of the feature subsets that were chosen is d. The complete set that the ants travelled through has a dimension of D. When the chosen feature subset is input, FPR stands for the false positive rate of classification and is defined as equation (10):

$$FPR = \frac{FP}{TN+FP} \quad (10)$$

The number of negative samples that the classifier misclassified as positive samples is known as FP. TN is the quantity of negative samples that the classifier properly identified. In other words, the false positive rate (FPR) is the ratio of the total number of negative samples to the number of classification error-free samples. When F is smaller for the fitness function, the chosen feature subset is better and satisfies the feature selection criterion.

Moreover, the co-evolution mechanism, pheromone update strategy, pheromone diffusion mechanism, and a hybrid strategy of the function are the foundations of the IACO algorithm model. The IACO algorithm's steps include; first separate the optimization problem into a number of smaller problems, with each smaller problem corresponding to a different subpopulation. The number of ants (k), pheromone quantity (Q), maximum number of iterations (T), parameter (αandβ), volatility coefficient (ρ), etc. are some of these parameters of the function. Additionally, each ant's starting position is chosen at random, and each subpopulation carries out the search procedure on its own. In each subpopulation of the system, locally update the pheromone concentration of the ants' passed path. In order to avoid falling into the local optimal value, it will assist to improve the convergence rate.

3.6 Classification:

Following feature dimension reduction, the selected features are fed into the LSTM for precise recognition of remote sensing characters. After using an LSTM classifier to choose useful features, the system's ability to detect and classify scenes in remote sensing images was improved. Furthermore, it has the default behavior of keeping data in memory for a long time. When neural networks are used in LULC classification, a large number of remote sensing photos are required to get better results. The LSTM classifier has already shown itself to be the most effective option when compared to other neural networks. The LSTM classifier is frequently composed of several LSTM units that retain the function's temporal quasi-periodic characteristics for extracting long-term and short-term dependencies. When in an overfit state, the neural network is unable to perform to its full capacity; this may hold true in the case of the LSTM. Every iteration, Dropout randomly chooses some LSTM units and sets their output to zero. While some of the other LSTM units are ignored and only used when error back propagation calculations must be made, the output value of a select few LSTM units is employed when calculating the error value. As a result, it will contribute to improving the system's ability to classify visual scenes using remote sensing data.

4 Results and Discussion:

The proposed IACO-LSTM is tested using the dataset that was described above. The experiments are performed on two public-domain databases, namely the Aerial Image Detection (AID) database. WHU-RS datasets and output images are utilized to construct the results, and the method is done using MATLAB R2020 software. The system configuration used for this research is an i5 processor with 8GB of RAM. The suggested improved ant colony optimization selection algorithm depends on the correctness of the corrections for accuracy, precision, recall, and F1 score. It performs best with LSTM classifiers of the function. The mentioned signal datasets are created and labelled manually as components of a framework. The total number of characters in labelled ligature images is counted and compared to the performance metric recognized, as shown in equations (11)– (14).

Accuracy

The accuracy performance metric, which is simply the ratio of correctly predicted observations to all observations.

The equation for accuracy is shown in Equation (11)

$$Accuracy = \frac{TP+TN}{TP+TN+FP+FN} \quad (11)$$

Precision

Precision is the ratio of correctly predicted observations to all predicted positive observations in terms of positive observations.

The equation for precision is shown in Equation (12)

$$Precision = \frac{TP}{TP+FP} \times 100 \qquad (12)$$

Recall

Recall determines how many Actual Positives our model actually captures by classifying it as Positive (True Positive).

The equation for Recall is shown in Equation (13)

$$Recall = \frac{TP}{TP+FN} \times 100 \qquad (13)$$

F1-Score

The F1 Score is calculated as the weighted average of Precision and Recall. As a result, when determining this score, both false positives and false negatives are taken into account.

The equation for F1-score is shown in the equation (14)

$$F - Score = \frac{2TP}{2TP+FP+FN} \times 100 \qquad (14)$$

4.1 Performance analysis of FCN ResNet-50 method:

The detection and classification performance of the IACO-LSTM using aerial image detection and WHU-RS datasets are discussed in this section. The proposed improved Ant colony optimization algorithm achieved an effective remote image classification accuracy of 96.79%, whereas the individual features such as accuracy, specificity, sensitivity, recall, and F1-Score of the datasets were lower. From the results, it is known that the combined set of features provides better classification accuracy than the individual features. Additionally, the performance of the Improved Ant Colony Optimization Method helped to improve the effectiveness of detection and classification by using remote sensing images. The IACO-LSTM method uses long-short-term memory for classifying the remote sensing scene images of the function.

The performance of the Improved Ant Colony Method is analyzed with different classifiers and with different feature selections. The different classifiers used to evaluate the proposed method are residual dense networks, support vector machines, and CNN, respectively. Moreover, the performance evaluation of two different remote sensing datasets with various classifiers is evaluated, as shown in Table 1. and Figure 6 shows the graphical comparison of the AID with various sensing images with different accuracy features. From the analysis, it is concluded that the LSTM classifiers achieve higher classification accuracy (91.79% for AID and WHU-RS, respectively) than the others.

Performance metrics	**Accuracy**	**Precision**	**Recall**	**F1 Score**
NN	82.51625	83.84689	83.83936	82.93755
RNN	82.64775	85.55038	85.54928	76.76766
GAN	80.56202	80.69679	82.93133	88.62092
DNN	81.60648	82.33227	78.90875	89.58426
Proposed	91.79838	90.60889	90.52582	91.1492

Table 2. Analysis belonging to AID datasets without feature selection

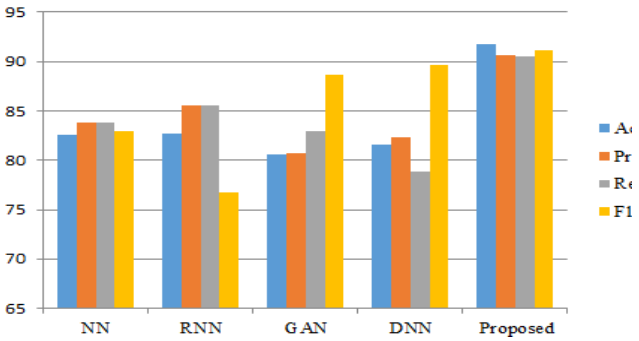

Figure 6. Graphical comparison of the AID datasets without feature selection

The performance analysis of IACO-LSTM with feature selection and different feature dimension reduction approaches is provided in Table 2. Figure 7 shows a graphical comparison of the LSTM with different classifiers. From the analysis, it is concluded that the proposed IACO-LSTM provides a higher classification accuracy of 96.79% than the RNN, NN, GAN, and DNN approaches. Figure 7 shows a graphical comparison of the LSTM with different classifiers. From the analysis, it is concluded that the proposed IACO-LSTM provides a higher classification accuracy of 96.79% than the RNN, NN, GAN, and DNN approaches. The IACO-LSTM provides higher accuracy (96.79%) because of optimal feature selection.

Performance metrics	Accuracy	Precision	Recall	F1 Score
NN	89.51625	90.84689	90.83936	82.93755
RNN	82.64775	91.55038	85.54928	86.76766
GAN	88.56202	87.69679	82.93133	88.62092
DNN	88.60648	86.33227	88.90875	89.58426
Proposed	96.79838	95.60889	97.52582	96.1492

Table 3: Analysis belonging to AID datasets with feature selection

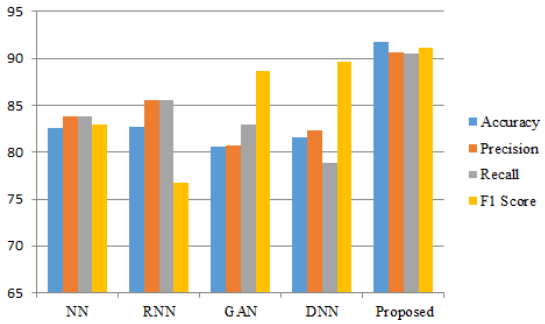

Figure 7 Graphical comparison of the AID datasets with feature selection

Optimization Algorithm	Accuracy	Precision	Recall	F1 Score
PSO	89.4587625	90.43579978	90.5678394	82.93755104
FFO	89.64774844	92.78550377	92.5492766	91.76765834
ACO	88.57645202	89.96791975	88.1313334	86.62091922
Proposed IACO	96.79838349	95.60889214	97.5258222	96.14919925

Table 4. Graphical comparison of the AID datasets with various optimization algorithm

The performance analysis of IACO-LSTM in the WHU-RS dataset without feature selection and with different feature dimension reduction approaches is provided in Table 4. Figure 8 shows a graphical comparison of the LSTM with different classifiers. From the analysis, it is concluded that the proposed IACO-LSTM provides a higher classification accuracy of 86.79% than the RNN, NN, GAN, and DNN approaches. The IACO-LSTM provides higher accuracy for WHU-RS dataset without feature selection and with different feature dimension reduction approaches is provided in Table 4. Figure 8 shows a graphical comparison of the LSTM with different classifiers. From the analysis, it is concluded that the proposed IACO-LSTM provides a higher classification accuracy of 86.79% than the RNN, NN, GAN, and DNN approaches. The IACO-LSTM provides higher accuracy (96.79%) because of optimal feature selection.

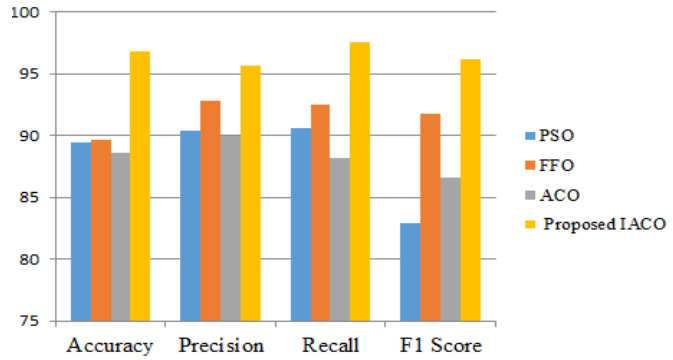

Figure 8:Graphical comparison of the WHU- RS datasets without feature selection

Performance metrics	Accuracy	Precision	Recall	F1 Score
NN	70.51625045	78.84688689	79.8393607	72.93755104
RNN	72.64774844	86.55037724	75.54927663	76.76765834
GAN	78.56201928	77.69679197	72.93133338	77.62091922
DNN	78.60647915	76.33227211	78.90875163	77.5842627
Proposed	86.79838349	84.60889214	85.52582223	86.76491992

Table 5: Analysis belonging to WHU – RS datasets without Feature selection

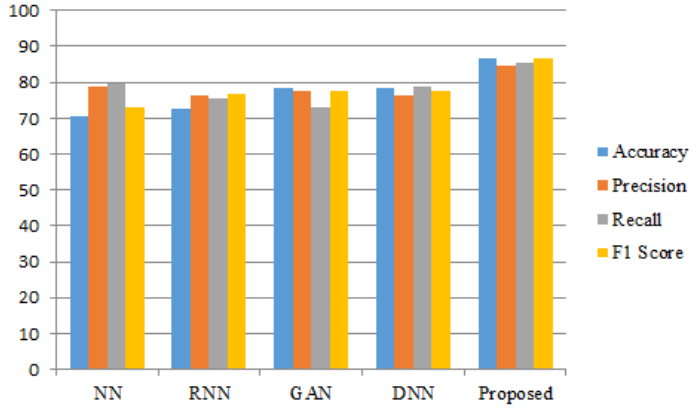

Figure 9Graphical comparison of the WHU – RS datasets with feature selection

Performance metrics	Accuracy	Precision	Recall	F1 Score
NN	89.51625045	84.84688689	89.8393607	82.93755104
RNN	82.64774844	86.55037724	85.54927663	86.76765834
GAN	88.56201928	87.69679197	82.93133338	87.62091922
DNN	88.60647915	86.33227211	88.90875163	87.5842627
Proposed	94.79838349	92.60889214	90.52582223	92.14919925

Table 6: Analysis belonging to WHU - RS datasets with Feature selection

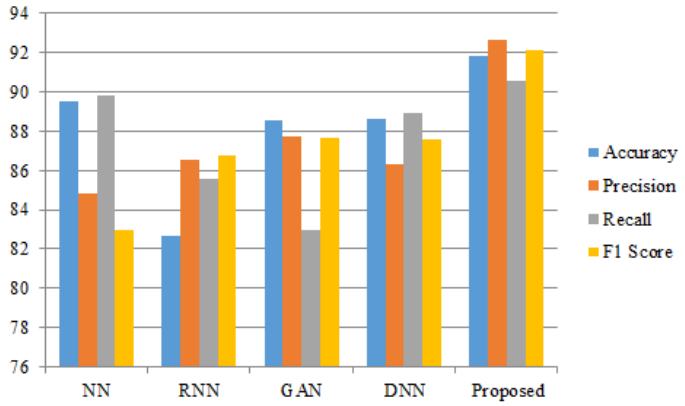

Figure 10: Graphical comparison of the WHU – RS datasets with various optimization algorithms.

Optimization Algorithm	Accuracy	Precision	Recall	F1 Score
PSO	89.4587625	90.43579978	90.56783936	82.93755104
FFO	89.64774844	90.78550377	90.54927663	91.76765834
ACO	88.57645202	89.96791975	88.13133338	86.62091922
Proposed IACO	91.79838349	92.60889214	91.52582223	92.14919925

Table 7. Analysis belonging to WHU – RS datasets with various optimization algorithms

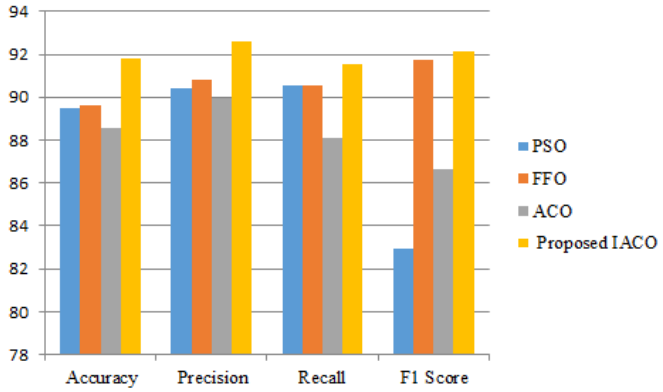

Figure 11: Graphical comparison of the WHU – RS datasets with proposed IACO algorithm

Dataset	**Accuracy**	**Precision**	**Recall**	**F1-Score**
AID – UCM Database [17]	94.1563	93.845	NA	NA
WHU- RS with UCM Database [18]	87.5%	NA	NA	NA
AID Database [19]	94.29%	NA	NA	NA
Proposed AID- WHU-RS Database	96.79838	95.60889	97.52582	96.1492

Table 8: comparison of proposed method with different databases

5 Conclusion: In this research, different algorithms are proposed to effectively detect the sensing images and classify the function. The first proposed method is "Improved Ant Colony Optimization," in which the Ant colony optimization is the accelerated version of the Ant nodes and helps to reduce the time required for feature selection, classification, and description of the identification process. Additionally, the unwanted or irrelevant features can be eliminated or selected to select the optimum feature values. By utilizing these feature values, the abnormality and normality of effective sensing images were extracted using an improved ant colony optimization algorithm. The identification results obtained were evaluated by means of measures such as recognition accuracy, precision, recall, and the F1-score of the system. The proposed method improved the identification accuracy (AID-WHU-RS) of the effective detection and classification of the function's remote sensing scene image by 96.79%.

References:

[1] Li, P., Chen, P. and Zhang, D., 2022. Cross-Modal Feature Representation Learning and Label Graph Mining in a Residual Multi-Attentional CNN-LSTM Network for Multi-Label Aerial Scene Classification. *Remote Sensing*, *14*(10), p.2424.

[2] Machado, G., Ferreira, E., Nogueira, K., Oliveira, H., Brito, M., Gama, P.H.T. and dos Santos, J.A., 2020. AiRound and CV-BrCT: Novel multiview datasets for scene classification. *IEEE Journal of Selected Topics in Applied Earth Observations and Remote Sensing*, *14*, pp.488-503.

[3] Rajagopal, A., Joshi, G.P., Ramachandran, A., Subhalakshmi, R.T., Khari, M., Jha, S., Shankar, K. and You, J., 2020. A deep learning model based on multi-objective particle swarm optimization for scene classification in unmanned aerial vehicles. *IEEE Access*, *8*, pp.135383-135393.

[4] Gómez, P. and Meoni, G., 2021. MSMatch: Semisupervised Multispectral Scene Classification with Few Labels. *IEEE Journal of*

Selected Topics in Applied Earth Observations and Remote Sensing, *14*, pp.11643-11654.

[5] Sen, O. and Keles, H.Y., 2020. On the evaluation of CNN models in remote-sensing scene classification domain. *PFG–Journal of Photogrammetry, Remote Sensing and Geoinformation Science*, *88*(6), pp.477-492.

[6] Torres, R.N. and Fraternali, P., 2021. Learning to identify illegal landfills through scene classification in aerial images. *Remote Sensing*, *13*(22), p.4520.

[7] Bi, Q., Qin, K., Zhang, H., Li, Z. and Xu, K., 2020. RADC-Net: A residual attention based convolution network for aerial scene classification. *Neurocomputing*, *377*, pp.345-359.

[8] Chen, S.B., Wei, Q.S., Wang, W.Z., Tang, J., Luo, B. and Wang, Z.Y., 2021. Remote sensing scene classification via multi-branch local attention network. *IEEE Transactions on Image Processing*, *31*, pp.99-109.

[9] Deepan, P. and Sudha, L.R., 2020. Remote sensing image scene classification using dilated convolutional neural networks. *International Journal*, *8*(7).

[10] Xu, K., Huang, H. and Deng, P., 2021. Remote sensing image scene classification based on global–local dual-branch structure model. *IEEE Geoscience and Remote Sensing Letters*, *19*, pp.1-5.

[11] Joshi, G.P., Alenezi, F., Thirumoorthy, G., Dutta, A.K. and You, J., 2021. Ensemble of deep learning-based multimodal remote sensing image classification model on unmanned aerial vehicle networks. *Mathematics*, *9*(22), p.2984.

[12] Liu, Z., Dong, A., Yu, J., Han, Y., Zhou, Y. and Zhao, K., 2022. Scene classification for remote sensing images with self- attention augmented CNN. *IET Image Processing*.

[13] Deng, P., Huang, H. and Xu, K., 2020. A Deep Neural Network Combined With Context Features for Remote Sensing Scene Classification. *IEEE Geoscience and Remote Sensing Letters*, *19*, pp.1-5.

[14] Xu, X., Chen, Y., Zhang, J., Chen, Y., Anandhan, P. and Manickam, A., 2021. A novel approach for scene classification from remote sensing images using deep learning methods. *European Journal of Remote Sensing*, *54*(sup2), pp.383-395.

[15] Su, Y., Zhong, Y., Zhu, Q. and Zhao, J., 2021. Urban scene understanding based on semantic and socioeconomic features: From high-resolution remote sensing imagery to multi-source geographic datasets. *ISPRS Journal of Photogrammetry and Remote Sensing*, *179*, pp.50-65.

[16] Zhao, X., Zhang, J., Tian, J., Zhuo, L. and Zhang, J., 2020. Residual dense network based on channel-spatial attention for the scene classification of a high-resolution remote sensing image. *Remote Sensing*, *12*(11), p.1887.

[17] Cao, R., Fang, L., Lu, T. and He, N., 2020. Self-attention-based deep feature fusion for remote sensing scene classification. *IEEE Geoscience and Remote Sensing Letters*, *18*(1), pp.43-47.

[18] Bai, L., Liu, Q., Li, C., Zhu, C., Ye, Z. and Xi, M., 2021. A lightweight and multiscale network for remote sensing image scene classification. *IEEE Geoscience and Remote Sensing Letters*, *19*, pp.1-5.

[19] Anwer, R.M., Khan, F.S. and Laaksonen, J., 2021. Compact deep color features for remote sensing scene classification. *Neural Processing Letters*, *53*(2), pp.1523-1544.

[20] Zhao, Z., Li, J., Luo, Z., Li, J. and Chen, C., 2020. Remote sensing image scene classification based on an enhanced attention module. *IEEE Geoscience and Remote Sensing Letters*, *18*(11), pp.1926-1930.

[21] M. Verma, N. Gupta, B. Tolani and R. Kaushal, "Explainable Custom CNN Architecture for Land Use Classification using Satellite Images," *2021 Sixth International Conference on Image Information Processing (ICIIP)*, Shimla, India, 2021, pp. 304-309, doi: 10.1109/ICIIP53038.2021.9702698

[22] Wang, M., Zhang, X., Niu, X. *et al.* Scene Classification of High-Resolution Remotely Sensed Image Based on ResNet. *J geovis spat anal* 3, 16, 2019.

[23] H. Wu, B. Liu, W. Su, W. Zhang and J. Sun, "Deep Filter Banks for Land-Use Scene Classification," in *IEEE Geoscience and Remote Sensing Letters*, vol. 13, no. 12, pp. 1895-1899, Dec. 2016.

[24] F. Zhang, B. Du and L. Zhang, "Saliency-Guided Unsupervised Feature Learning for Scene Classification," in *IEEE Transactions on Geoscience and Remote Sensing*, vol. 53, no. 4, pp. 2175-2184, April 2015.

[25] Q. Weng, Z. Mao, J. Lin and W. Guo, "Land-Use Classification via Extreme Learning Classifier Based on Deep Convolutional Features," in *IEEE Geoscience and Remote Sensing Letters*, vol. 14, no. 5, pp. 704-708, May 2017.

[26] M. Castelluccio, G. Poggi, C. Sansone and L. Verdoliva, Land use classification in remote sensing images by convolutional neural networks, 2015.

[27] F. Hu, G.-S. Xia, Z. Wang, X. Huang, L. Zhang, and H. Sun, "Unsupervised feature learning via spectral clustering of multidimensional patches for remotely sensed scene classification," IEEE Journal of Selected Topics in Applied Earth Observations and Remote Sensing, vol. 8, no. 5, pp. 2015–2030, may 2015

[28] Huang, L.; Chen, C.; Li, W.; Du, Q. Remote Sensing Image Scene Classification Using Multi-Scale Completed Local Binary Patterns and Fisher Vectors. *Remote Sens. 8*, 483, 2016.

[29] Chen, J.; Wang, C.; Ma, Z.; Chen, J.; He, D.; Ackland, S. Remote Sensing Scene Classification Based on Convolutional Neural Networks Pre-Trained Using Attention-Guided Sparse Filters. *Remote Sens.*, *10*, 290, 2018.

[30] Esam Othman, YakoubBazi, Naif Alajlan, HaikelAlhichri&FaridMelgani Using convolutional features and a sparse autoencoder for land-use scene classification, International Journal of Remote Sensing, 37:10, 2149-2167, 2016.